# Synthesis and Characterization of $Tb[N(CN)_2]_3 \cdot 2H_2O$ and $Eu[N(CN)_2]_3 \cdot 2H_2O$: Two New Luminescent Rare-Earth Dicyanamides

Abanti Nag,[†] Peter J. Schmidt,[‡] and Wolfgang Schnick*[,†]

*Lehrstuhl für Anorganische Festkörperchemie, Department Chemie und Biochemie, Ludwig-Maximilians-Universität (LMU) München, Butenandtstrasse 5-13 (D), D-81377 München, Germany, and Philips Research Laboratories, Weisshausstrasse 2, D-52066 Aachen, Germany*

*Received March 23, 2006. Revised Manuscript Received September 7, 2006*

Two new rare-earth dicyanamides, namely, $Tb[N(CN)_2]_3 \cdot 2H_2O$ and $Eu[N(CN)_2]_3 \cdot 2H_2O$, have been prepared by ion exchange in aqueous solution, followed by evaporation of the solvent at room temperature. The structures of both compounds have been solved and refined from single-crystal and powder X-ray diffraction data, respectively. The two compounds are isostructural and are built up from irregular quadratic antiprismatic $LnN_6O_2$ polyhedra connected to each other by three crystallographically independent dicyanamide ($[N(CN)_2]_3^-$) ions ($Tb[N(CN)_2]_3 \cdot 2H_2O$, $P2_1/n$, $Z = 4$, $a = 7.4632(15)$ Å, $b = 11.523(2)$ Å, $c = 13.944(3)$ Å, $\beta = 94.06(3)°$, $V = 1196.2(4)$ Å$^3$; $Eu[N(CN)_2]_3 \cdot 2H_2O$, $P2_1/n$, $Z = 4$, $a = 7.4780(3)$ Å, $b = 11.5429(5)$ Å, $c = 13.9756(7)$ Å, $\beta = 93.998(4)°$, $V = 1203.41(10)$ Å$^3$). Annealing of the hydrated phases of $Ln[N(CN)_2]_3 \cdot 2H_2O$ (Ln = Eu, Tb) at 150 °C under an argon atmosphere leads to the formation of nonhydrated $Ln[N(CN)_2]_3$ (Ln = Eu, Tb). Both the hydrated ($Eu[N(CN)_2]_3 \cdot 2H_2O$) and nonhydrated ($Eu[N(CN)_2]_3$) europium(III) dicyanamides show red luminescence due to the dominant intensity of $^5D_0-{}^7F_J$ ($J = 1, 2, 4$) emission lines by excitation at 365 nm. The broad excitation band of europium(III) dicyanamide (FWHM = 8000 cm$^{-1}$) ranging between 260 and 420 nm with $\lambda_{max} \approx 30000$ cm$^{-1}$ is ascribed to a Eu−N charge-transfer transition, which is significantly shifted to lower energy compared to that of oxo compounds due to the nephalauxetic effect. Similarly, both the hydrated ($Tb[N(CN)_2]_3 \cdot 2H_2O$) and nonhydrated ($Tb[N(CN)_2]_3$) terbium(III) dicyanamides show green emission at $\lambda_{exc} = 365$ nm, arising mainly from the dominant $^5D_0-{}^7F_4$ transition. However, unlike europium(III) dicyanamide, the broad excitation band of terbium(III) dicyanamide ranging between 250 and 400 nm with a maximum at 33000 cm$^{-1}$ can be assigned to the $4f^8-4f^75d^1$ transition of $Tb^{3+}$.

## Introduction

There is a growing interest in the development of new saturated-color-emitting materials that combine good mechanical, thermal, and chemical stability in air with high room-temperature emission quantum yields.[1−3] Inorganic materials involving integration of organic and inorganic components into the same compound, leading to formation of hybrid skeletons, can have a wide variety of unique applications.[4−7] In some cases, this increase in structural complexity gives rise to significant scientific and technological opportunities by combining attractive features of both components within a single material.[8] The association of molecular units with transition or rare-earth metals allows for the tuning of their electronic and magnetic properties due to the versatility of its coordination. Recently, a significant increase in the research of molecular materials in which metal ion centers are bridged through organic molecules has been observed, due to potential application in optoelectronics, magnetism, and catalysis.[9−11] There is an attempt to replace the traditional inorganic solid-state compounds in luminescent lighting and display devices by molecular materials, because of advantages such as mass production by solution processing or gas-phase deposition, potential flexibility by means of polymer-based packaging of such thin-film devices, and finally low cost.

As a fundamental class of compounds of special importance for molecular chemistry, cyanamides and dicyanamides have gained increasing attention within the past decade.[12,13]

* To whom correspondence should be addressed. E-mail: wolfgang.schnick@uni-muenchen.de.
[†] Ludwig-Maximilians-Universität München.
[‡] Philips Research Laboratories.

(1) Friend, R. H.; Gymer, R. W.; Holmes, A. B.; Burroughes, J. H.; Marks, R. N.; Taliani, C.; Bradley, D. D. C.; Dos Santos, D. A.; Bredas, J. L.; Logdlund, M.; Salaneck, W. R. *Nature* **1999**, *397*, 121.
(2) Cao, Y.; Parker, I. D.; Yu, G.; Zhang, C.; Heeger, A. J. *Nature* **1999**, *397*, 414.
(3) Jüstel, T.; Nikol, H.; Ronda, C. *Angew. Chem., Int. Ed.* **1998**, *37*, 3084.
(4) Gomez-Romero, P. *Adv. Mater.* **2001**, *13*, 163.
(5) Sauchez, C.; Lebeau, B.; Chaput, F.; Boilot, J. P. *Adv. Mater.* **2003**, *15*, 1969.
(6) Serre, C.; Pelle, F.; Gardant, N.; Férey, G. *Chem. Mater.* **2004**, *16*, 1177.
(7) Millange, F.; Serre, C.; Marrot, J.; Gardant, N.; Pellé, F.; Férey, G. *J. Mater. Chem.* **2004**, *14*, 642.
(8) Shunmugan, R.; Tew, G. N. *J. Am. Chem. Soc.* **2005**, *127*, 13567.
(9) Kim, J.; Chen, B.; Reineke, T. M.; Li, H.; Eddaoudi, M.; Moler, D. B.; O'Keeffe, M.; Yaghi, O. M. *J. Am. Chem. Soc.* **2001**, *123*, 8239.
(10) Eddaoudi, M.; Moler, D. B.; Li, H.; Chen, B.; Reineke, T. M.; O'Keeffe, M.; Yaghi, O. M. *Acc. Chem. Soc.* **2001**, *34*, 319.
(11) De Bettencourt-Dias, A. *Inorg. Chem.* **2005**, *44*, 2734.
(12) Batten, S. R.; Murray, K. S. *Coord. Chem. Rev.* **2003**, *246*, 103.
(13) Jürgens, B.; Irran, E.; Senker, J.; Kroll, P.; Müller, H.; Schnick, W. *J. Am. Chem. Soc.* **2003**, *125*, 10288.

10.1021/cm0607029 CCC: $33.50 
Published on Web 11/07/2006

In fact, a number of alkali-metal,[14−17] alkaline-earth-metal,[18−20] transition-metal,[21−25] and also main-group[26] cyanamides and dicyanamides were obtained following different synthetic routes. In this context, the dicyanamide anion ($[N{\equiv}C{-}N{-}C{\equiv}N]^-$) is considered to play an important role because of its variation in coordinating ability with metal ions by terminal and/or bridging nitrogen atoms, resulting in monodentate, bidentate, or even tridentate coordination. On the other hand, introduction of lanthanides within the hybrid skeleton may create an unusual architecture because of high and variable coordination of rare-earth ions and may also give unique properties stemming from their f−f electronic transitions owing to high chromaticity and long-lived excited states.[27] However, in the field of inorganic dicyanamides, most of the solids reported until now have been dicyanamide complexes containing lanthanide ions.[28] Only a very few rare-earth compounds have been described which contain Ln···N−CN bonds.[29−32] In an attempt to optimize lanthanide-centered emission in both the hydrated and nonhydrated lanthanide dicyanamides and to explore the mechanism of excitation and emission processes, we have prepared two new luminescent rare-earth dicyanamides, hydrated europium(III) dicyanamide ($Eu[N(CN)_2]_3 \cdot 2H_2O$) and hydrated terbium(III) dicyanamide ($Tb[N(CN)_2]_3 \cdot 2H_2O$) showing red and green emissions, respectively. The structures of both the hydrated compounds are isotypic and were solved from single-crystal and powder diffraction data, respectively. Also, the excitation and emission properties of isostructural nonhydrated europium(III) dicyanamide ($Eu[N(CN)_2]_3$) and nonhydrated terbium(III) dicyanamide ($Tb[N(CN)_2]_3$) are explored.

## Experimental Section

**Syntheses and Chemical Analysis.** $Ln[N(CN)_2]_3 \cdot 2H_2O$ (Ln = Eu, Tb) were prepared by ion exchange in aqueous solution at room temperature. A column containing 5 mL of a strongly acidic ion-exchange resin (Merck, Ionenaustauscher I, Art. 4765) with an ion exchange capacity of $1.7 \times 10^{-3}$ mol/mL was completely filled with a solution of 0.02 M $LnCl_3 \cdot 6H_2O$ (Alfa Aesar). The complete loading of $Ln^{3+}$ was indicated by the change of acidic to neutral pH, i.e., the pH of the $LnCl_3 \cdot 6H_2O$ solution. After the column was fully loaded, the exchange resin was washed thoroughly with deionized water, and the removal of excess chloride was substantiated by the $AgNO_3$ method. Subsequently, a solution of sodium dicyanamide ($Na[C_2N_3]$; Fluka, >96%) was poured onto the column, and the eluate was evaporated at room temperature. The concentration of sodium dicyanamide solution was varied from 0.01 to 0.5 M to obtain suitable single crystals for structure determination. Under these conditions, tiny colorless crystals of $Tb[N(CN)_2]_3 \cdot 2H_2O$ were obtained, allowing the structure determination of $Tb[N(CN)_2]_3 \cdot 2H_2O$ from single-crystal diffraction data. On the other hand, $Eu[N(CN)_2]_3 \cdot 2H_2O$ does not produce good single crystals under these conditions. Furthermore, other attempts for obtaining single crystals of $Eu[N(CN)_2]_3 \cdot 2H_2O$ by using other solvent systems as a crystallization medium or solute/vapor diffusion processes also failed. Hence, the structural parameters of $Eu[N(CN)_2]_3 \cdot 2H_2O$ were refined from powder diffraction data using the cell parameters and atomic coordinates of isostructural $Tb[N(CN)_2]_3 \cdot 2H_2O$ as the starting values. The nonhydrated $Eu[N(CN)_2]_3$ and $Tb[N(CN)_2]_3$ were obtained by annealing the corresponding hydrated phases in an ampule under argon to a temperature of 150 °C. Both the hydrated and nonhydrated phases are photostable and also stable in air. The initial characterization was carried out using powder X-ray diffraction, thermogravimetric analysis, and infrared spectroscopy.

Thermal analysis was performed on a simultaneous thermogravimetry/differential thermal analyzer (Setaram thermoanalyzer TGA 92-2400) in the temperature range 25−800 °C (heating rate 10 °C/min) in an argon atmosphere. Infrared spectra were recorded at room temperature using a Bruker IFS 66v/S FTIR spectrometer in the range 2000−400 $cm^{-1}$ by dispersing the sample in anhydrous KBr pellets. Diffuse reflectance spectra of the powder samples were recorded between 200 and 700 nm with a Varian Cary 500 spectrophotometer. Excitation and emission spectra were obtained at room temperature using a spectrofluorometer FL900 (Edinburgh Instruments) with a Xe lamp as a light source fitted with a Hamamatsu photomultiplier. The excitation and emission spectra presented are corrected for the FL900 spectrometer sensitivity and excitation lamp characteristics.

The quantum efficiency (QE) is defined as the ratio of the number of emitted quanta to the number of absorbed quanta. The QE values of unknown phosphors were determined in comparison with those of standard phosphors, the efficiencies of which were reported previously. The quantum efficiencies ($QE_{sample}$) of the unknown phosphors were calculated using the equation[33,34]

$$QE_{sample} = \left(\frac{1 - R_{std}}{1 - R_{sample}}\right)\left(\frac{\int I_{sample}}{\int I_{std}}\right) QE_{std} \qquad (1)$$

where $QE_{std}$ is the quantum efficiency of the standard phosphor, $R_{std}$ and $R_{sample}$ are the amounts of exciting radiation reflected by the standard and by the sample, respectively, and $\int I_{std}$ and $\int I_{sample}$ are the integrated emission intensities for the standard and sample phosphor, respectively. The values of $R_{std}$, $R_{sample}$, $\int I_{std}$, and $\int I_{sample}$ are obtained under identical conditions such as sample weight,

(14) Becker, M.; Nuss, J.; Jansen, M. *Z. Anorg. Allg. Chem.* **2000**, *626*, 2505.
(15) Jürgens, B.; Irran, E.; Schneider, J.; Schnick, W. *Inorg. Chem.* **2000**, *39*, 665.
(16) Becker, M.; Jansen, M. *Solid State Sci.* **2000**, *2*, 711.
(17) Irran, E.; Jürgens, B.; Schnick, W. *Chem.−Eur. J.* **2001**, *7*, 5372.
(18) Berger, U.; Schnick, W. *J. Alloys Compd.* **1994**, *206*, 179.
(19) Jürgens, B.; Irran, E.; Schnick, W. *J. Solid State Chem.* **2001**, *157*, 241.
(20) Irran, E.; Jürgens, B.; Schmid, S.; Schnick, W. *Z. Anorg. Allg. Chem.* **2005**, *631*, 1512.
(21) Batten, S. R.; Jensen, P.; Kepert, C. J.; Kurmoo, M.; Moubaraki, B.; Murray, K. S.; Price, D. J. *J. Chem. Soc., Dalton Trans.* **1999**, 2987.
(22) Manson, J. L.; Kmety, C. R.; Epstein, A. J.; Miller, J. S. *Inorg. Chem.* **1999**, *38*, 2552.
(23) Jensen, P.; Price, D. J.; Batten, S. R.; Moubaraki, B.; Murray, K. S. *Chem.−Eur. J.* **2000**, *6*, 3186.
(24) Jürgens, B., Irran, E.; Höppe, H. A.; Schnick, W. *Z. Anorg. Allg. Chem.* **2004**, *630*, 219.
(25) Liu, X.; Müller, P.; Dronskowski, R. *Z. Anorg. Allg. Chem.* **2005**, *631*, 1071.
(26) Jürgens, B.; Höppe, H. A.; Schnick, W. *Solid State Sci.* **2002**, *4*, 821.
(27) Cotton, F. A.; Wilkinson, G.; Murillo, C. A.; Bochmann, M. *Advanced Inorganic Chemistry*, 6th ed.; John-Wiley & Sons: New York, 1999.
(28) Wu, A.-Q.; Zheng, F.-K.; Chen, W.-T.; Cai, L.-Z.; Guo, G.-C.; Huang, J.-S.; Dong, Z.-C.; Takano, Y. *Inorg. Chem.* **2004**, *43*, 4839.
(29) Hashimoto, Y.; Takahashi, M.; Kikkawa, S.; Kanamaru, F. *J. Solid State Chem.* **1995**, *114*, 592.
(30) Reckeweg, O.; DiSalvo, F. J. *Z. Anorg. Allg. Chem.* **2003**, *629*, 177.
(31) Srinivasan, R.; Ströbele, M.; Meyer, H.-J. *Inorg. Chem.* **2003**, *42*, 3406.
(32) Nag, A.; Schnick, W. *Z. Anorg. Allg. Chem.* **2006**, *632*, 609.
(33) Bril, A. In *Luminescence of Organic and Inorganic Materials*, Kallman, H. P., Spruch, G. M., Eds.; Wiley & Sons: Eindhoven, The Netherlands, 1962.
(34) Jüstel, T.; Krupa, J. C.; Wiechert, D. U. *J. Lumin.* **2001**, *93*, 179.

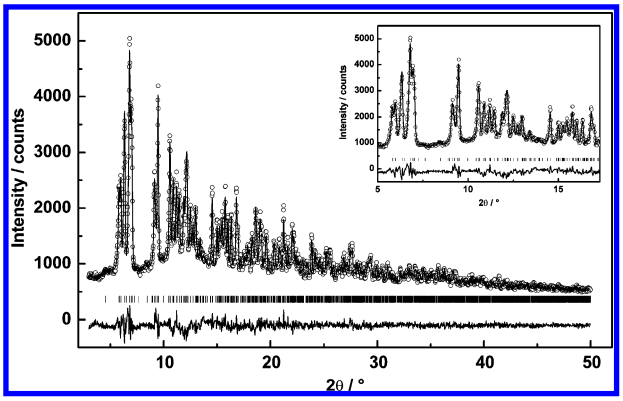


**Figure 1.** Final Rietveld refinement plot for $Eu[N(CN)_2]_3 \cdot 2H_2O$. Observed (open circles), calculated (line), and difference profiles of the X-ray powder diffraction are plotted on the same scale. Bragg peaks are indicated by vertical lines for $Eu[N(CN)_2]_3 \cdot 2H_2O$. An enlargement of the low-angle range is represented in the inset.

instrument settings (excitation and emission slit widths), temperature (room temperature), and excitation wavelength. The standard phosphors which were used are Philips U744 ($Y_2O_3$:$Eu^{3+}$, QE = 84% for 254 nm excitation) and Lumogen red from BASF (perylene dye, QE = 42.3% for 365 nm excitation) for $Eu^{3+}$ samples and Philips U763 ($LaPO_4$:$Ce^{3+}$,$Tb^{3+}$, QE = 90% for 254 nm excitation) $SrSi_2N_2O_2$:Eu from Philips (QE = 81.3% for 365 nm excitation) for $Tb^{3+}$ samples.

For the calculation of CIE (Commission Internationale d'Eclairage) color coordinates ($x$, $y$), the emission spectra were weighted by the 10° standard observer CIE color matching functions. After summarizing, the obtained tristimulus values were normalized to obtain CIE 1933 color coordinates.

**Structure Determination.** The ion exchange synthesis of $Ln[N(CN)_2]_3 \cdot 2H_2O$ led to isolated single crystals of $Tb[N(CN)_2]_3 \cdot 2H_2O$ and microcrystalline powdered samples of $Eu[N(CN)_2]_3 \cdot 2H_2O$. Single-crystal structure determination of $Tb[N(CN)_2]_3 \cdot 2H_2O$ was performed at room temperature on an ENRAF-NONIUS Kappa CCD diffractometer equipped with a rotating anode producing graphite-monochromated Mo Kα radiation ($\lambda$ = 0.71073 Å). The reflections were corrected for Lorentz and polarization effects. A semiempirical absorption correction using $\psi$ scans was applied. The space group could be unambiguously determined as $P2_1/n$ (No. 14). The crystal structure was solved by direct methods using the software package SHELXS-97[35] and refined using the full-matrix least-squares method implemented in SHELXL-97[36] with anisotropic displacement parameters for all non-hydrogen atoms. The positions of the hydrogen atoms of the crystal water molecule could also be determined from difference Fourier maps and refined isotropically. Details of the structure determination are given in Table 1. Atomic coordinates and bond distances and angles are provided in the Supporting Information.

For X-ray diffraction investigation of $Eu[N(CN)_2]_3 \cdot 2H_2O$, powders of the samples were enclosed in glass capillaries with a diameter of 0.3 mm. The measurements were carried out in Debye–Scherrer geometry on a STOE Stadi P powder diffractometer with Ge(111)-monochromatized Mo Kα radiation ($\lambda$ = 0.7093 Å). The X-ray diffractometry study indicates that the diffraction pattern of $Eu[N(CN)_2]_3 \cdot 2H_2O$ could be indexed with lattice constants similar to those of $Tb[N(CN)_2]_3 \cdot 2H_2O$ and the same space group as $Tb[N(CN)_2]_3 \cdot 2H_2O$; these compounds were found to be isotypic (Figure 1). Hence, the Rietveld refinements were performed with the program GSAS[37] using the atomic coordinates of $Tb[N(CN)_2]_3 \cdot 2H_2O$ as the starting values. To describe the profile of the X-ray reflections, a pseudo-Voigt function with special symmetry was used.[38] Details of the structure determination are summarized in Table 2. Further details of the crystal structure investigations are available from the Fachinformationszentrum Karlsruhe, D-76344 Eggenstein-Leopoldshafen, Germany, e-mail crysdata@FIZ-karlsruhe.de, on quoting the depository numbers CSD-416308

**Table 1. Crystallographic Data and Structure Refinement of $Tb[N(CN)_2]_3 \cdot 2H_2O$**

| | |
|---|---|
| formula | $Tb[N(CN)_2]_3 \cdot 2H_2O$ |
| mol wt | 393.1 |
| cryst syst | monoclinic |
| space group | $P2_1/n$ (No. 14) |
| $T$/K | 293 |
| diffractometer | Kappa CCD |
| radiation ($\lambda$/Å) | Mo Kα (0.71073) |
| $a$/Å | 7.4632(15) |
| $b$/Å | 11.523(2) |
| $c$/Å | 13.944(3) |
| $\beta$/deg | 94.06(3) |
| $V$/Å$^3$ | 1196.2(4) |
| $Z$ | 4 |
| $\rho_{calcd}$/g·cm$^{-3}$ | 2.183 |
| $F$(000) | 736 |
| $\mu$/mm$^{-1}$ | 5.923 |
| cryst size/mm$^3$ | 0.11 × 0.09 × 0.06 |
| diffraction range | $3.1 \le \theta \le 27.48$ |
| index range | $-9 \le h \le +9$, $-14 \le k \le +14$, $-18 \le l \le +17$ |
| total no. of reflns | 19462 |
| no. of independent reflns | 2723 |
| no. of independent reflns | 1992 ($R_{int}$ = 0.0370) |
| no. of refined params | 177 |
| corrections | absorption, Lorentz, polarization |
| abs correction | multiscan |
| min/max transm ratio | 0.530/0.691 |
| min/max residual electron density/e·Å$^{-3}$ | −0.302/0.585 |
| GOF | 1.025 |
| final $R$ indices [$I > 2\sigma(I)$] | $R1$ = 0.0193, $wR2$ = 0.0376 |
| $R$ indices (all data) | $R1$ = 0.0334, $wR2$ = 0.0419 with $w = [\sigma^2(F_o^2) + (0.0000P)^2 + 0.4464P]^{-1}$ where $P = (F_o^2 + 2F_c^2)/3$ |

**Table 2. Crystallographic Data Structure Refinement of $Eu[N(CN)_2]_3 \cdot 2H_2O$**

| | |
|---|---|
| formula | $Eu[N(CN)_2]_3 \cdot 2H_2O$ |
| mol wt | 386.15 |
| cryst syst | monoclinic |
| space group | $P2_1/n$ (No. 14) |
| radiation ($\lambda$/Å) | Mo Kα (0.7093) |
| $a$/Å | 7.4780(4) |
| $b$/Å | 11.5429(5) |
| $c$/Å | 13.9756(7) |
| $\beta$/Å | 93.998(4) |
| $V$/Å$^3$ | 1203.41(10) |
| $Z$ | 4 |
| $\rho_{calcd}$/g·cm$^{-3}$ | 2.131 |
| profile range | $3 \le 2\theta \le 50$ |
| no. of data points | 4699 |
| no. of positional params | 66 |
| no. of profile params | 19 |
| $R$ values | $R_F^2$ = 0.08029 |
| | $wR_P$(fit) = 0.0467 |
| | $R_P$(fit) = 0.0368 |
| | $wR_P$(back) = 0.0513 |
| | $R_P$(back) = 0.0392 |

(35) Sheldrick, G. M. *SHELXS-97, Program for solution of crystal structures*; University of Göttingen: Göttingen, Germany, 1997.
(36) Sheldrick, G. M. *SHELXL-97, Program for refinement of crystal structures*; University of Göttingen: Göttingen, Germany, 1997.
(37) Larson, A. C.; von Dreele, R. B. *General structure analysis system*; Report LAUR 86-748; Los Alamos National Laboratory: Los Alamos, NM, 1994.
(38) Finger, L. W.; Cox, D. E.; Jephcoat, A. P. *J. Appl. Crystallogr.* **1994**, *27*, 892.

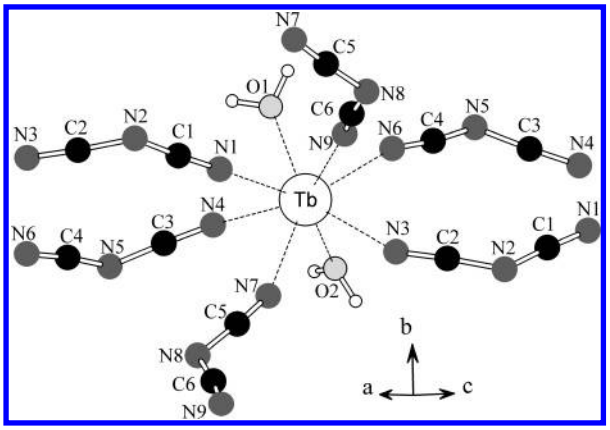


**Figure 2.** Coordination modes of $Tb^{3+}$ in $Tb[N(CN)_2]_3 \cdot 2H_2O$.

$(Tb[N(CN)_2]_3 \cdot 2H_2O)$ and CSD-416309 $(Eu[N(CN)_2]_3 \cdot 2H_2O)$ and the name of the author(s) and citing the paper.

## Results and Discussion

Both $Tb[N(CN)_2]_3 \cdot 2H_2O$ and $Eu[N(CN)_2]_3 \cdot 2H_2O$ are isostructural and crystallize in the monoclinic space group $P2_1/n$. Furthermore, $Tb[N(CN)_2]_3 \cdot 2H_2O$ and $Eu[N(CN)_2]_3 \cdot 2H_2O$ are also isostructural with previously reported $Gd[N(CN)_2]_3 \cdot 2H_2O$.[32] The lanthanide ions (Tb, Eu) are eight-coordinated as is displayed with a complete coordination sphere in Figure 2. The polyhedron around Ln(III) can be described as an irregular quadratic antiprism. Each lanthanide ion is surrounded by six nitrogen atoms coming exclusively from three crystallographically independent dicyanamide ions ($[N(CN)_2]^-$). There are two water molecules completing the coordination sphere of the lanthanide ion. The interatomic distances are close to those usually reported for rare-earth-(III) solids; Tb/Eu−N distances vary from 2.45 to 2.48 Å, and Tb/Eu−O distances are between 2.38 and 2.40 Å. The dicyanamides coordinate to $Ln^{3+}$ only by the terminal N atoms (N1, N3, N4, N6, N7, and N9), resulting in a bidentate terminal coordination. The angles (N−C≡N, 173−175°; C−N−C, 118−122°) and bond distances (terminal C≡N, 1.14−1.15 Å; bridging N−C, 1.29−1.30 Å) of the dicyanamide ions are similar to those of other dicyanamides.[39] The site symmetry of the dicyanamide ion $[N{\equiv}C{-}N{-}C{\equiv}N]^-$ is reduced to $C_1$ because of slightly different bond lengths C≡N and angles N−C≡N.

Figure 3 shows the polyhedral representation of $Tb[N(CN)_2]_3 \cdot 2H_2O$. It exhibits a three-dimensional network built up from eight-coordinated lanthanide ions forming $LnO_2N_6$ polyhedra. These units are connected to each other through the dicyanamide moieties. This arrangement of six dicyanamide groups around the lanthanide ion leads to a structure of two-dimensional sheets. The metal ions in two adjacent sheets are approximately 8 Å apart. These layers interact with each other through $\pi-\pi$ stacking as well as through hydrogen bonding. There are four O−H···N hydrogen bonds, two of them running to terminal N atoms (N7 and N9 with O−N distances of 3.1636 and 3.196 Å, respectively) and two to the bridging N atoms (N2 and N8 with O−N distances of 2.8219 and 2.9121 Å, respectively) of dicyanamide ions.

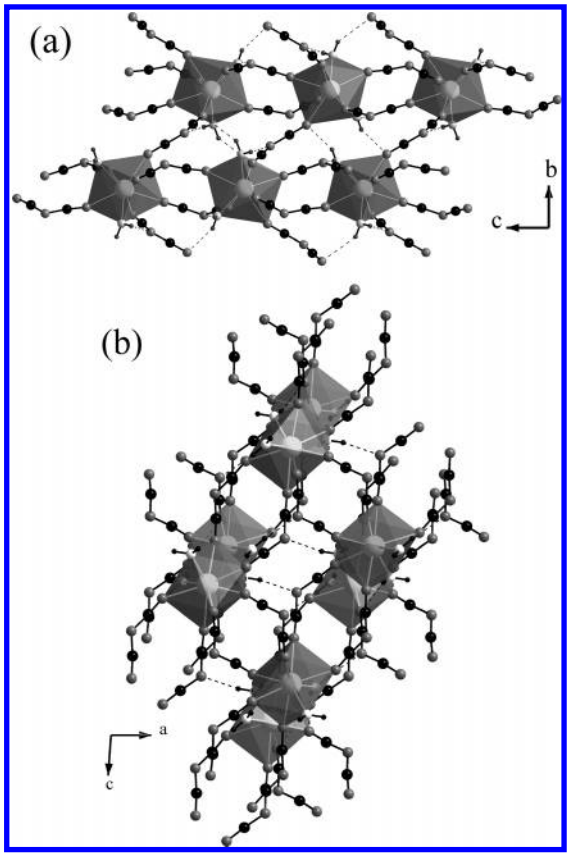


**Figure 3.** Polyhedral representation of the structure of $Tb[N(CN)_2]_3 \cdot 2H_2O$ along the (a) *a* axis and (b) *b* axis. Terbium, carbon, nitrogen, oxygen, and hydrogen are represented as large white spheres, large black spheres, gray spheres, small white spheres, and small black spheres, respectively.

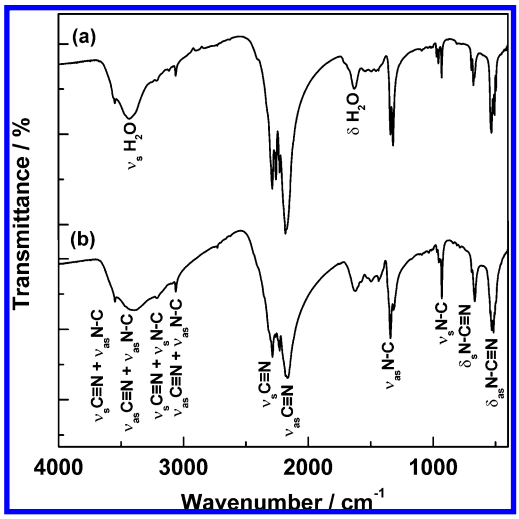


**Figure 4.** Infrared spectra of (a) $Tb[N(CN)_2]_3 \cdot 2H_2O$ and (b) $Eu[N(CN)_2]_3 \cdot 2H_2O$.

The infrared spectra of $Ln[N(CN)_2]_3 \cdot 2H_2O$ (Ln = Tb, Eu) clearly show the presence of the vibrational bands characteristic for C≡N and N−C as shown in Figure 4, confirming the presence of the dicyanamide group within the solids.[40] Additionally, the broad band between 3600 and 3000 $cm^{-1}$ and sharp signal at 1610 $cm^{-1}$ originate from the stretching

(39) Jürgens, B.; Irran, E.; Schnick, W. *J. Solid State Chem.* **2005**, *178*, 72.

(40) Jürgens, B.; Milius, W.; Morys, P.; Schnick, W. *Z. Anorg. Allg. Chem.* **1998**, *624*, 91.

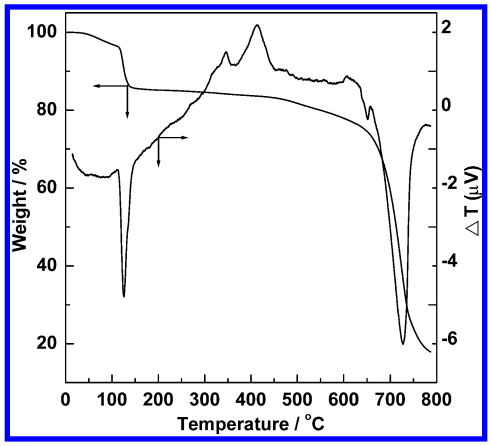


**Figure 5.** TG/DTA curve of $Tb[N(CN)_2]_3 \cdot 2H_2O$ recorded under an argon atmosphere at a heating rate of 10 °C/min.

and bending vibrations of water molecules, confirming the presence of $H_2O$ group in $Ln[N(CN)_2]_3 \cdot 2H_2O$ (Ln = Tb, Eu).

The thermal stability of $Ln[N(CN)_2]_3 \cdot 2H_2O$ (Ln = Tb, Eu) has been studied using thermogravimetric/differential thermal analysis (TG/DTA). Since $Ln[N(CN)_2]_3 \cdot 2H_2O$ contains water molecules, structural changes at higher temperatures were expected for this compound. The TG/DTA measurements, performed between 20 and 800 °C, have shown identical results for both compounds with two weight losses (Figure 5). The initial weight loss of 15% in the range of 100−150 °C corresponds to the loss of adsorbed water and lattice water, and the second weight loss of 60% in the range of 450−750 °C corresponds to the loss of organic moieties. These are also indicated by the two endothermic effects of the DTA curve at 120 and 725 °C, respectively. The dehydration of $Ln[N(CN)_2]_3 \cdot 2H_2O$ occurs at 150 °C, leading to the formation of anhydrous $Ln[N(CN)_2]_3$, the structure of which shows the removal of water molecules and the rearrangement of dicyanamide groups.[39] The crystallinity of the compound is kept after the first structural change. The crystallinity remains up to 350 °C, indicating the thermal stability of the compounds. Above 400 °C, the decomposition of dicyanamide is indicated by the exothermic effect of the DTA curve, leading to the formation of an X-ray amorphous powder which at higher temperature converts to the corresponding oxides.

The nonhydrated $Ln[N(CN)_2]_3$ (Ln = Eu, Tb) are isostructural with other lanthanide dicyanamides, the structure of which has been previously reported by Jürgens et al.[39] The nonhydrated phases crystallize with orthorhombic symmetry having space group *Cmcm*. In the crystal structure there are two crystallographically independent dicyanamide ions ($[N(CN)_2]^-$) which are coordinated with $Ln^{3+}$. The $Ln^{3+}$ ions are coordinated by three bridging N atoms and six terminal N atoms of the dicyanamide ions, forming a tricapped trigonal prism of $LnN_9$ polyhedra.

It has been demonstrated for inorganic molecular compounds that the luminescence of the trivalent rare earths might arise because of absorption in the ligand group followed by intramolecular transfer of energy from the lowest excited triplet state that is populated via intersystem crossing from the excited singlet state involving the ligand-to-metal charge-transfer (LMCT) state in lanthanide compounds.

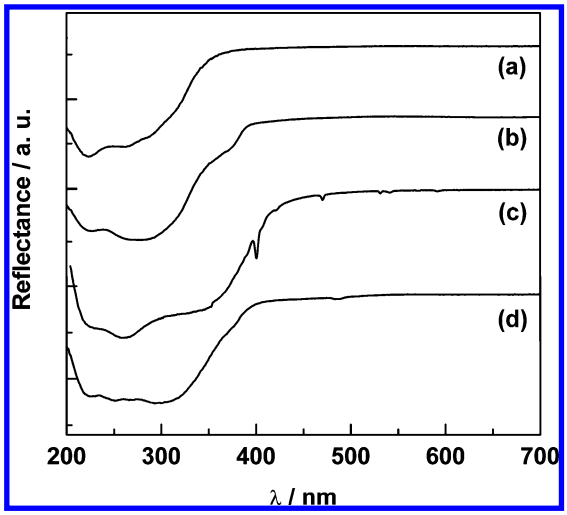


**Figure 6.** Diffuse reflectance spectra at room temperature of $Ln[N(CN)_2]_3 \cdot 2H_2O$: (a) $La[N(CN)_2]_3 \cdot 2H_2O$, (b) $Gd[N(CN)_2]_3 \cdot 2H_2O$, (c) $Eu[N(CN)_2]_3 \cdot 2H_2O$, and (d) $Tb[N(CN)_2]_3 \cdot 2H_2O$.

There are two methods of energy transfer; one is intramolecular energy transfer between 4f states of the lanthanide ion and the LMCT state, and the other one is the intramolecular energy transfer between ligand states (singlet and triplet) and the LMCT state. The theory developed by Faustino et al.[41] and experimentally confirmed by Carlos et al.[42] estimates that the energy transfer through the ligand−LMCT state transfer process is the dominant case by several orders of magnitude over that through the former lanthanide ion−LMCT state transfer process. To find whether the LMCT states take part in the excitation−emission process of $Ln[N(CN)_2]_3 \cdot 2H_2O$, the diffuse reflectance spectra are recorded for $Ln[N(CN)_2]_3 \cdot 2H_2O$ (Ln = La, Eu, Gd, Tb) at room temperature (Figure 6). Furthermore, the arithmetic difference between the diffuse reflectance spectra of isostructural $Eu^{3+}$ and $Gd^{3+}$ compounds allows for the explicit identification of low-lying LMCT states for $Eu^{3+}$, since for $Gd^{3+}$ the energy difference between the first excited state and the fundamental levels is too high to allow the detection of a charge-transfer state in the UV−vis range. The effects of LMCT states on the $Eu^{3+}$ emission quantum yield have recently been described in a notable theoretical approach that modeled the intramolecular LMCT state−4f levels and LMCT state−ligand energy-transfer processes. Numerical estimates for the luminescence quenching via LMCT−$Eu^{3+}$ energy transfer show that when the LMCT state lies approximately between 10000 and 20000 $cm^{-1}$, quenching is extremely high (emission quantum yields close to zero), corresponding to the exhaustion of the $^5D_0$ and $^5D_1$ level populations. The diffuse reflectance spectrum of lanthanum dicyanamide consists of a broad band in the UV region with maxima at 220 and 280 nm (Figure 6a). Apart from a shoulder around 370 nm, the absorption spectrum of $Gd[N(CN)_2]_3 \cdot 2H_2O$ shows features similar to those of the lanthanum dicyanamide spectrum (Figure 6b). The shoulder in the spectrum of $Gd[N(CN)_2]_3 \cdot 2H_2O$ might be appearing

(41) Faustino, W. M.; Malta, O. L.; de Sá, G. F. *J. Chem. Phys.* **2005**, *122*, 0544109.
(42) Carlos, L. D.; Fernandes, J. A.; Sá Ferreira, R. A.; Malta, O. L.; Gonçalves, I. S.; Ribeiro-Claro, P. *Chem. Phys. Lett.* **2005**, *413*, 22.

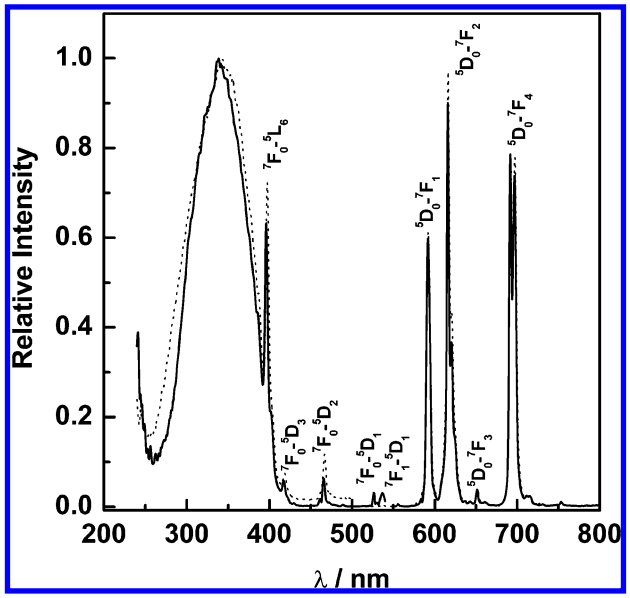


**Figure 7.** Excitation ($\lambda_{em}$ = 616 nm) and emission ($\lambda_{exc}$ = 365 nm) spectra of $Eu[N(CN)_2]_3 \cdot 2H_2O$ (solid line) and $Eu[N(CN)_2]_3$ (dotted line).

due to some impurities since it is not observed in lanthanum dicyanamide and also isostructural $Tb[N(CN)_2]_3 \cdot 2H_2O$ (Figure 6d). Furthermore, the absorption band at 220 nm remains unchanged for all the lanthanide dicyanamides and is also observed in the case of $Na[N(CN)_2]$, indicating that this absorption might correspond to transition in the dicyanamide ligands. The diffuse reflectance spectrum of $Eu[N(CN)_2]_3 \cdot 2H_2O$ consists of a very broad absorption band extending from 200 to 400 nm and a sharp line at 395 nm which can be attributed to $^7F_0-^5L_6$ intra-$4f^6$ transition. The absorption bands around the 220−300 nm region are very similar to those observed in the spectra of other lanthanide dicyanamides $Ln[N(CN)_2]_3 \cdot 2H_2O$ (Ln = La, Gd, Tb). Furthermore, absorption at a wavelength around 340 nm has no correspondence in the spectra of $La^{3+}$, $Gd^{3+}$, or $Tb^{3+}$ and is therefore ascribed to a Eu−N charge-transfer transition. However, the diffuse reflectance spectrum of $Eu[N(CN)_2]_3 \cdot 2H_2O$ does not show the presence of a low-lying LMCT band overlapping with the $^5D_0$ and $^5D_1$ levels of $Eu^{3+}$, which in turn ruled out the quenching of $Eu^{3+}$ luminescence by a nonradiative process through low-energy LMCT states.[43]

Figure 7 shows the room-temperature excitation (PLE) and emission (PL) spectra of hydrated $Eu[N(CN)_2]_3 \cdot 2H_2O$ and nonhydrated $Eu[N(CN)_2]_3$. The emission spectrum of $Eu[N(CN)_2]_3 \cdot 2H_2O$, recorded at $\lambda_{exc}$ = 365 nm, is composed of the typical $Eu^{3+}$ intra-$4f^6$ emission lines which can be assigned to transitions between the first excited state ($^5D_0$) and the ground multiplets ($^7F_{0-4}$). However, the presence of all the multiplets in the emission lines due to $2J + 1$ Stark components of *J*-degeneracy splitting cannot be well resolved due to room-temperature measurements except for the 2-fold degeneracy of the $^5D_0-^7F_2$ line as well as the 2-fold degeneracy of the $^5D_0-^7F_4$ line. Furthermore, the $^5D_0-^7F_1$ line is known to originate from magnetic dipole transition, while the $^5D_0-^7F_2$ and $^5D_0-^7F_4$ lines originate from electric dipole transitions.[44] According to the Judd−Ofelt theory,[45,46] the magnetic dipole transition is permitted while the electric dipole transition is forbidden. The latter are allowed only for the condition that the $Eu^{3+}$ ions occupy a site without an inversion center and are sensitive to local symmetry. In the case of europium dicyanamide, the electric dipole transition is much stronger than the magnetic dipole transition, suggesting that $Eu^{3+}$ occupies a low-symmetry site without an inversion center. Moreover, Malta et al.[47−49] theoretically calculated the intensity parameters of $^5D_0-^7F_2$ and $^5D_0-^7F_4$ transitions in the $Eu^{3+}$ complex taking into account the forced electric dipole and dynamic coupling mechanism and using magnetic dipole allowed $^5D_0-^7F_1$ as a reference (as it does not depend on the local ligand field) and interpreted the high experimental intensity of the $^5D_0-^7F_2$ line as a consequence of the hypersensitive behavior, pointing to a highly polarizable chemical environment around the $Eu^{3+}$ ion.

The excitation spectrum (PLE), monitored at $\lambda_{em}$ = 612 nm, the most intense emission line of $Eu^{3+}$, exhibits a large broad band between 260 and 420 nm, with a maximum at around 335 nm, superimposed with sharp peaks centered at wavelengths extending from 390 to 550 nm. The sharp peaks can be attributed to inner 4f shell $^7F_0-^5L_6$ (395 nm), $^7F_0-^5D_3$ (417 nm), $^7F_0-^5D_2$ (465 nm), $^7F_0-^5D_1$ (525 nm), and $^7F_1-^5D_1$ (538 nm) transitions of $Eu^{3+}$.[50] The broad excitation spectra of the trivalent rare-earth ions can be ascribed to either (i) charge-transfer transitions ($4f^n \rightarrow 4f^{n+1}L^{-1}$, where L = ligand) or (ii) $4f^n \rightarrow 4f^{n-1}5d$ transitions. Charge-transfer transitions are found for rare-earth ions which like to be reduced, whereas 4f−5d transitions are observed for the rare earth ions which like to be oxidized. Hence, the broad band in the case of europium dicyanamides can only be ascribed to originate from Eu−N charge-transfer (CT) transitions, i.e., the electron transfer from nitrogen to the $Eu^{3+}$ ion because it is easy to reduce $Eu^{3+}$ to $Eu^{2+}$ in the excited state. The full width at half-maximum (8000 $cm^{-1}$) of the Eu−N charge-transfer band is quite comparable with that of the Eu−O charge-transfer band in oxide lattices; however, the position of the Eu−N charge-transfer band is significantly shifted to lower energies compared to that of the oxo compounds. The charge-transfer band of Eu−F in $YF_3$:$Eu^{3+}$ appears around 150 nm (66000 $cm^{-1}$), whereas in the case of $Y_2O_3$:$Eu^{3+}$, the charge-transfer band of Eu−O is shifted to longer wavelength and appears around 250 nm (40000 $cm^{-1}$). Therefore, one can expect a red shift of the Eu−N charge-transfer transition band around 335 nm (30000 $cm^{-1}$) due to the nephelauxetic effect; i.e., with increasing covalency (F < O < N) the interaction between the electrons is reduced since they spread out over wider orbitals, and hence,

(43) De Mello Donegá, C.; Ribeiro, S. J. L.; Gonçalves, R. R.; Blasse, G. *J. Phys. Chem. Solids* **1996**, *57*, 1727.
(44) Görller-Walrand, C.; Binnemans, K. In *Handbook on the Physics and Chemistry of Rare-earths*, Gschneider, K. A., Jr., Eyring, L., Eds.; North Holland: Amsterdam, 1998; Vol. 25, Chapter 167.
(45) Judd, B. R. *Phys. Rev.* **1962**, *127*, 750.
(46) Ofelt, G. S. *J. Chem. Phys.* **1962**, *37*, 511.
(47) Malta, O. L.; Couto dos Santos, M. A.; Thompson, L. C.; Ito, N. K. *J. Lumin.* **1996**, *69*, 77.
(48) Malta, O. L.; Brito, H. F.; Menezes, J. F. S.; Gonçalves e Silva, F. R.; Alves, S., Jr.; Farias, F. S., Jr.; de Andrade, A. V. M. *J. Lumin.* **1997**, *75*, 255.
(49) Carlos, L. D.; Messaddeq, Y.; Brito, H. F.; Sá Ferreira, R. A.; de Zea Bermudez, V.; Ribeiro, S. J. L. *Adv. Mater.* **2000**, *12*, 594.
(50) Dieke, G. H. *Spectra and Energy Levels of Rare-Earth Ions in Crystals*; Interscience Publishers: New York, 1968.

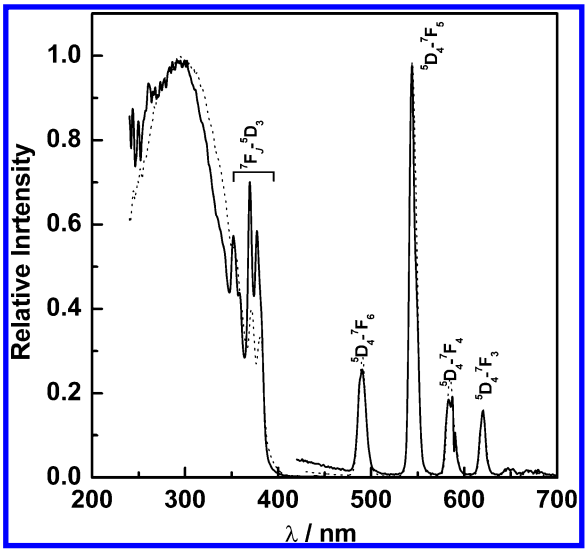


**Figure 8.** Excitation ($\lambda_{em}$ = 545 nm) and emission ($\lambda_{exc}$ = 365 nm) spectra of $Tb[N(CN)_2]_3 \cdot 2H_2O$ (solid line) and $Tb[N(CN)_2]_3$ (dotted line).

the energy required to remove an electron from a ligand atom decreases in the order F > O > N, which in turn shifts the electronic transitions toward lower energies (Eu−N < Eu−O < Eu−F).[51] Moreover, the excitation spectrum of the nonhydrated $Eu[N(CN)_2]_3$ shows features similar to those of the spectrum of the hydrated compound except for a slight shift (∼10 nm) of the excitation maximum toward longer wavelength (348 nm), indicating that excitation mechanisms are essentially the same for both the hydrated and nonhydrated phases. The slight shift toward the longer wavelength can be attributed to the different crystal structures of hydrated and nonhydrated europium(III) dicyanamides. Further, the red shift of the charge-transfer band of hydrated versus nonhydrated europium(III) dicyanamides is also to be expected due to the more covalent environment around $Eu^{3+}$ in nonhydrated $Eu[N(CN)_2]_3$ with $EuN_9$ polyhedra. On the other hand, the emissions of hydrated and nonhydrated $Eu[N(CN)_2]_3$ arise from intra-$4f^6$ $^5D_0-{}^7F_J$ ($J = 0-4$) transitions of $Eu^{3+}$, which are not very sensitive to the local environment as the 4f orbital is well shielded by the 5s and 5p orbitals. Only the $^5D_0-{}^7F_2$ transition depends on the local environment of $Eu^{3+}$ and therefore is called a hypersensitive transition. Closer inspection of the emission spectra of hydrated and nonhydrated europium dicyanamide (Figure 7) reveals an increase in intensity of the $^5D_0-{}^7F_2$ line in the case of nonhydrated $Eu[N(CN)_2]_3$ compared to the hydrated compound.

Figure 8 shows the excitation (PLE) and emission (PL) spectra of $Tb[N(CN)_2]_3 \cdot 2H_2O$ and $Tb[N(CN)_2]_3$. The excitation spectrum of $Tb[N(CN)_2]_3 \cdot 2H_2O$, monitored at $Tb^{3+}$ green emission at 545 nm ($^5D_4-{}^7F_5$), mainly consists of a wide band from 250 to 400 nm with a maximum at 300 nm superimposed with sharp lines around 370 nm. The sharp lines originate from intra-4f transitions of $Tb^{3+}$. However, unlike europium dicyanamide, the broad band at 33000 $cm^{-1}$ (fwhm ≈ 9000 $cm^{-1}$) in the excitation spectra of the Tb compounds cannot be ascribed to a Tb−N charge-transfer transition, which is expected to be located at much higher energy because of the formation of unstable divalent lanthanides such as $Tb^{2+}$ in the excited states. Hence, the broad band can only be ascribed to an f−d transition of $Tb^{3+}$. The structure of the f−d excitation spectra could be explained by crystal-field and spin−orbit interactions for the 5d electron and the Coulomb interaction between the 4f and 5d electrons giving rise to splitting between the low-spin (LS) and high-spin (HS) states. The excitation of one "inner" f state to an "outer" d state can be regarded as the first step of the removal of the electron and thus produces stable tetravalent rare-earth ions such as $Tb^{4+}$, which is expected to have a lower energy than the corresponding charge-transfer state, which in turn forms unstable divalent $Tb^{2+}$. The ground configuration of the $Tb^{3+}$ ion is $4f^8$. The excited configuration is $4f^75d^1$, in which the 4f shell is half-filled. Because the lowest excited 4f level within the $4f^7$ configuration is located at very high energy (32000 $cm^{-1}$ for $Gd^{3+}$), the f−d excitation spectrum of $Tb^{3+}$ is expected to be quite similar to that of $Ce^{3+}$ ($4f^0$-$5d^1$ configuration in the excited state) showing a band corresponding to the different 5d states. The $4f^8-4f^75d$ transition of $Tb^{3+}$ is generally observed in a relatively higher energy region in the case of fluoride or oxide compounds.[52,53] In the present case, a lower energy shift of f−d transitions can be expected due to the nephelauxetic effect. In fact, in the case of $Ce^{3+}$ a low-energy excitation band is observed even in oxide lattices.[54] Therefore, the broad excitation band of $Tb[N(CN)_2]_3 \cdot 2H_2O$ as well as $Tb[N(CN)_2]_3$ can be explained as the $4f^8-4f^75d$ transition of $Tb^{3+}$. Excitation into the $4f^8-4f^75d$ transition of $Tb^{3+}$ at 300 nm yields the characteristic $^5D_4-{}^7F_J$ ($J = 3-6$) emission of $Tb^{3+}$, with $^5D_4-{}^7F_5$ green emission as the most intense one ($\lambda_{max}$ = 545 nm). Similar to $Eu[N(CN)_2]_3$, nonhydrated $Tb[N(CN)_2]_3$ also shows a red shift (∼10 nm) in the excitation maximum compared to hydrated $Tb[N(CN)_2]_3 \cdot 2H_2O$, which can be explained as different local symmetries of $Tb^{3+}$ between hydrated and nonhydrated compounds due to different crystal structures and coordination, which in turn affects the energy of the d orbital, resulting in excitation maxima at longer wavelengths.

The CIE color coordinates ($x$, $y$) of $Eu[N(CN)_2]_3 \cdot 2H_2O$ (0.633, 0.359), $Eu[N(CN)_2]_3$ (0.638, 0.356), $Tb[N(CN)_2]_3 \cdot 2H_2O$ (0.319, 0.509), and $Tb[N(CN)_2]_3$ (0.334, 0.568) are quite comparable to those of commercial red- and green-emitting phosphors, respectively.

The quantum efficiencies were measured for both hydrated and nonhydrated phases under monitoring wavelengths of 256 and 365 nm to compare these two phosphors with standard lamp phosphors. The quantum efficiencies described here are overall quantum efficiencies of the luminescent materials. For $Eu[N(CN)_2]_3 \cdot 2H_2O$, the standard phosphor $Y_2O_3$:Eu powder (from Philips) with a QE of 84% for 254 nm excitation and 84.5% absorption was used as a reference. For this excitation wavelength, the Eu(III) emission of $Eu[N(CN)_2]_3 \cdot 2H_2O$ is completely quenched. Similar is the case

(51) Blasse, G.; Grabmeier, B. C. *Luminescent Materials*, Springer-Verlag: Berlin, Heidelberg, 1998.

(52) Ning, L.; Mak, C. S. K.; Tanner, P. A. *Phys. Rev. B* **2005**, *72*, 085127.
(53) van Pieterson, L.; Reid, M. F.; Burdick, G. W.; Meijerink, A. *Phys. Rev. B* **2002**, *65*, 045114.
(54) Nag, A.; Kutty, T. R. N. *Mater. Chem. Phys.* **2005**, *91*, 524.

for nonhydrated $Eu[N(CN)_2]_3$. For an excitation wavelength of 365 nm, $Eu[N(CN)_2]_3 \cdot 2H_2O$ shows a QE of 6% compared to standard Lumogen red, a perylene dye (from BASF) which has a QE of 42.3%. In the case of nonhydrated $Eu[N(CN)_2]_3$ the QE increased to 10.5%. In the case of $Tb[N(CN)_2]_3 \cdot 2H_2O$, the commercial phosphor $LaPO_4$:Ce,Tb powder (from Philips) with a quantum efficiency of 90% for 254 nm excitation and 96.7% absorption was used as a reference. The sample $Tb[N(CN)_2]_3 \cdot 2H_2O$ showed 95.2% absorption of the excitation light and a quantum efficiency of 15.7%. For an excitation wavelength of 365 nm, $Tb[N(CN)_2]_3 \cdot 2H_2O$ shows a QE of 18% compared to standard $SrSi_2N_2O_2$:Eu (from Philips), which has a QE of 81.3%. In the case of nonhydrated $Tb[N(CN)_2]_3$ the QE increased to 25.4%. The QE study clearly shows that the hydrated phases exhibit comparatively lower efficiencies than the corresponding nonhydrated phases. It is well-known that the nonradiative effect of the OH oscillators of the $H_2O$ molecule affects the luminescence features of the trivalent lanthanides.[55] Therefore, comparatively low quantum efficiencies of hydrated dicyanamides can be explained with nonradiative losses due to multiphonon emission involving the water molecules. In addition, strong concentration quenching might be expected due to energy transfer between two adjacent $Tb^{3+}$ or $Eu^{3+}$ ions in $Tb[N(CN)_2]_3 \cdot 2H_2O$ or $Eu[N(CN)_2]_3 \cdot 2H_2O$, respectively. However, the Eu−Eu or Tb−Tb distance within a layer is about 8 Å, which ruled out the energy migration through exchange interaction (critical distance ($R_c$) ≤5 Å), resulting in strong concentration quenching.[51] Only weak multipolar interaction can occur between two $Tb^{3+}$ or $Eu^{3+}$ ions in $Tb[N(CN)_2]_3 \cdot 2H_2O$ or $Eu[N(CN)_2]_3 \cdot 2H_2O$, respectively. On the other hand, at higher concentrations of the activators there is also a possibility of cross-relaxation in which the higher energy level emissions of $Tb^{3+}$ or $Eu^{3+}$ can be quenched. The low-energy excitation maxima of terbium or europium dicyanamide open up the possibility to develop white LEDs in combination with blue GaN-based LEDs and lanthanide carbon nitrides, which is a developing field of research in the present day.[3] However, a better efficiency can be obtained by further shifting the excitation maxima toward longer wavelength to achieve better energy overlap between the emission spectrum of a blue GaN-based LED and the excitation spectra of rare-earth-based phosphors. This can be obtained by tailoring the ligands of lanthanide carbon nitride compounds, which is presently in progress. Furthermore, an attempt has been made to prepare isostructural $Gd[N(CN)_2]_3 \cdot 2H_2O$ doped with $Eu^{3+}$ or $Tb^{3+}$. However, doping is not effective in this case as the hydrated phases are prepared by ion exchange in aqueous solution and the nonhydrated phases are obtained by heat treatment of the hydrated phases at 150 °C, which is very low compared to the temperature of the diffusion-controlled high-temperature solid-state reactions. Therefore, the resulting product yields heterogeneous mixtures of two phases of gadolinium dicyanamides and europium or terbium dicyanamides, respectively, even at a very low concentration of dopants, and the resulting emission intensities of the compounds are extremely low due to the presence of a nonemissive $Gd[N(CN)_2]_3$ phase.

## Conclusions

The synthesis, structure, and characterization of new rare-earth dicyanamides have been accomplished. The presence of a rare earth and molecular units such as $[N(CN)_2]_3^-$ resulted in low-energy excitation bands yielding efficient red and green emission from $Eu^{3+}$ and $Tb^{3+}$, respectively. Other similar compounds are currently under investigation to explore the emission by tailoring the ligand to shift the excitation wavelength suitable for applications in lighting and display devices.

**Acknowledgment.** We thank Dr. P. Mayer for single-crystal data collection and J. Kechele and A. Sattler for conducting the TG/DTA measurement (all Department of Chemistry and Biochemistry of LMU Munich), and H. Ohland (Philips Research) for luminescence measurements. Financial support by the Deutsche Forschungsgemeinschaft (Schwerpunktprogramm "Lanthanoidspezifische Funktionalitäten in Molekül und Material", Project SCHN 377/10-2) and the Fonds der Chemischen Industrie is gratefully acknowledged.

**Supporting Information Available:** X-ray crystallographic information files (CIFs) for $Tb[N(CN)_2]_3 \cdot 2H_2O$ and $Eu[N(CN)_2]_3 \cdot 2H_2O$ and tables of atomic coordinates, anisotropic displacement parameters, and bond lengths and angles for $Tb[N(CN)_2]_3 \cdot 2H_2O$ and diffuse reflectance spectrum of sodium dicyanamide (PDF). This material is available free of charge via the Internet at http://pubs.acs.org.

CM0607029

(55) Supkowski, R. M.; Horrocks, W. D., Jr. *Inorg. Chim. Acta* **2002**, *340*, 44.